Numerical Simulation of Turbulent Flows using the SST-SAS Model

MAURO GRIONI[1,2], SERGIO ELASKAR[1,3,4], PASCAL BRUEL[5], ANIBAL MIRASSO[2]
[1]National Scientific and Technical Research Council (CONICET),
ARGENTINA

[2]Institute of Structural Mechanics and Seismic Risk,
Research and teaching staff, Faculty of Engineering,
National University of Cuyo,
Mendoza 5500,
ARGENTINA

[3]Department of Aeronautical, Faculty of Exact, Physical and Natural Sciences,
National University of Córdoba,
Córdoba 5000,
ARGENTINA

[4]Institute of Advanced Studies in Engineering and Technology (IDIT),
National University of Córdoba,
Córdoba 5000,
ARGENTINA

[5]CNRS,
University Pau & Pays Adour, LMAP, Inria Cagire Team,
Avenue de l'Université, 64013 Pau,
FRANCE

Abstract: - Turbulent flows play a crucial role in various engineering and scientific applications, and the accurate prediction of these flows remains a challenging task. This review explores the application of the Shear Stress Transport Scale-Adaptive Simulation (SST-SAS) turbulence model for solving incompressible turbulent flows, with a specific focus on unsteady wakes behind bluff bodies. Providing a concise overview of the model's formulation and its advantages, this article highlights the efficacy of the SST-SAS model in simulating the intricate dynamics in different configurations of circular cylinders. The present study affirms that the SST-SAS model can be considered a highly viable alternative for simulating unsteady flows around bluff bodies due to the good predictive quality of the resulting simulations.

Key-Words: - SST-SAS turbulence model, unsteady flow, interference effects, wall proximity, tandem circular cylinders, staggered tube bundle, wall-mounted cylinder.

Received: January 22, 2023. Revised: November 13, 2023. Accepted: December 12, 2023. Published: January 29, 2024.

1 Introduction

It is widely acknowledged that for quite a broad range of flow configurations, the Reynolds-Averaged Navier-Stokes (RANS) approach can yield relatively satisfactory results for mean flow quantities at a moderate computational cost. However, in scenarios of flows largely dominated by large-scale separation, the standard RANS methodology finds rapidly its limits. Under such conditions, the intricate nature of turbulent flows calls for alternative modeling techniques to obtain more accurate numerical predictions. In the last decade, significant strides have been made in Large Eddy Simulation (LES) models but their systematic application to specific industrial flows at very high Reynolds and Rayleigh numbers remains quite a challenge, [1]. The hybridization of LES with RANS is one possibility that permits to strike a balance between the results' accuracy and computational efficiency, [2]. Revisiting the RANS

framework and reevaluating the derivation of its governing equations was another option followed in [3], to develop an unsteady RANS (URANS) model called the scale-adaptive simulation (SAS) approach. More specifically, the SAS version called SST-SAS [4], and based on the k–ω SST RANS model, [5], became quite a popular choice when it comes to selecting a turbulence model. Indeed, a search through the literature of the last ten-year period with the keyword "SST-SAS" in the title or the abstract returns more than one hundred references. The diversity of flow configurations dealt with is quite impressive, a glimpse of it is given by the references listed below:

- Canonical configurations: flows over a backward-facing step [6]; the periodic hill [7]; flows past a circular cylinder [8], [9], [10], [11], [12]; flows past two circular cylinders [13]; the flow past a prismatic bluff body [14]; twin impinging jets [15].
- Systems of practical interest: the flow around a high-speed train [16], the flow past an airfoil [17]; the flow over a wall mounted array of cubes [11]; the flow in a tube bundle [18], [19]; flows in centrifugal pumps [7], [20]; the flow in a pressure wave exchanger [21]; the filling of a tank [22]; a ship air wake [23]; flows in Francis turbines [24], [25], [26].

In the above-listed studies, the SST-SAS method was employed either with commercial codes (ANSYS-FLUENT, CFX, STAR-CCM+) or with the open-source library OpenFOAM or in-house codes. But, regardless of the kind of numerical set-up used, the SST-SAS turbulence model is generally praised for its capability of well-predicting on relatively coarse meshes the mean flow properties while being able to resolve a significant portion of the flow temporal fluctuations. It should be noted though that in most of these studies, the assessment of the quality of the model is largely based on visual comparisons with experimental data and not on the recourse to objective criteria. Some studies are performing such a comparison on integral flow quantities but only two studies are using objective criteria to compare experimental and numerical data sets, [14], [18]. The context regarding the use of the SAS approach being now recalled, the objective of the present contribution is i) to review published applications of the SST-SAS model to the simulation of incompressible unsteady flow over cylinder(s) and ii) to present new results obtained for the configuration of the flow over a wall-mounted cylinder. Such configurations hold practical relevance in various engineering applications, including heat exchangers, pipelines used in fuel storage and distribution chains, and offshore and ocean structures like subsea pipelines, marine risers, and platform legs. The paper is organized as follows: Section 2 describes the governing equations and the SST-SAS turbulence model. In Section 3, the reviewed cases are analyzed and discussed. Section 4 presents recent experimental and numerical results for the flow around a wall-mounted cylinder. Finally, Section 5 presents the concluding remarks along with some axes of future activity.

2 Background

2.1 Flow Model Formulation

The behavior of fluids in motion is comprehensively described by the Navier-Stokes and continuity equations. The ensemble averaging of these equations, considering a constant density, isothermal, and incompressible body force-free flow, yields the Unsteady Reynolds-Averaged Navier-Stokes (URANS) equations. In the Cartesian coordinate system (O, x_1, x_2, x_3), these equations can be expressed as follows:

$$\frac{\partial \langle u_i \rangle}{\partial x_i} = 0 \tag{1}$$

$$\frac{\partial \langle u_i \rangle}{\partial t} + \frac{\partial \langle u_i \rangle \langle u_j \rangle}{\partial x_j} = \frac{1}{\rho}\frac{\partial \langle p \rangle}{\partial x_j} + \frac{\partial}{\partial x_j}\left[\upsilon \left(\frac{\partial \langle u_i \rangle}{\partial x_j} + \frac{\partial \langle u_j \rangle}{\partial x_i} \right) - \langle u_i' u_j' \rangle \right] \tag{2}$$

where $\langle u_i \rangle$ is the ensemble average component of the velocity in the direction x_i, ρ is the density of the fluid, $\langle p \rangle$ is the ensemble average pressure, υ is the kinematic viscosity and $\langle u_i' u_j' \rangle$ is the Reynolds stress tensor. To complete this URANS system, the Reynold stress tensor, representing turbulence effects through nonlinear terms, is modeled through a Boussinesq-like relation, namely:

$$\langle u_i' u_j' \rangle = -\upsilon_t \left(\frac{\partial \langle u_i \rangle}{\partial x_j} + \frac{\partial \langle u_j \rangle}{\partial x_i} \right) + \frac{2}{3} k \delta_{ij} \tag{3}$$

where the turbulent eddy viscosity υ_t and the turbulence kinetic energy k are calculated thanks to the recourse to the SST-SAS turbulence model.

2.2 SST-SAS Two-Equation Turbulence Model

Menter and co-authors developed the Scale Adaptive Simulation (SAS) method [3], [27], [28] to simulate turbulent flows by using a two-equation model. When the SAS approach is coupled with the k-ω SST model [5], it yields the SST-SAS turbulence model [3], [4], [29], [30]. The resulting equations for k and ω are given by:

$$\frac{\partial k}{\partial t}+\left\langle u_j\right\rangle\frac{\partial k}{\partial x_j}=P_k-\beta^* k\omega+\frac{\partial}{\partial x_j}\left[\Gamma_k\frac{\partial k}{\partial x_j}\right] \tag{4}$$

$$\frac{\partial \omega}{\partial t}+\left\langle u_j\right\rangle\frac{\partial \omega}{\partial x_j}=\frac{\gamma}{\mu_t}P_k-\beta\omega^2+\frac{\partial}{\partial x_j}\left[\Gamma_\omega\frac{\partial \omega}{\partial x_j}\right] + \left(1-F_1\right)\frac{2}{\sigma_{\omega,2}}\frac{1}{\omega}\frac{\partial k}{\partial x_j}\frac{\partial \omega}{\partial x_j}+Q_{SAS} \tag{5}$$

where F_1 is a blending function and P_k is the production term of turbulence kinetic energy given by $P_k=\upsilon_t S^2$ with $S=\sqrt{2S_{ij}S_{ij}}$ and $S_{ij}=\frac{1}{2}\left(\frac{\partial\left\langle u_i\right\rangle}{\partial x_j}+\frac{\partial\left\langle u_j\right\rangle}{\partial x_i}\right)$. The constant β^* is taken equal to 0.09 and $\sigma_{\omega,2}$ = 1.168 while the turbulent diffusivities are expressed as $\Gamma_k=\left(\upsilon+\frac{\upsilon_t}{\sigma_k}\right)$ and $\Gamma_\omega=\left(\upsilon+\frac{\upsilon_t}{\sigma_\omega}\right)$ where the value of σ_k and σ_ω, just like β, result from a mix between the constants of the k–ε and k–ω models. The SST-SAS model differs from the original SST model by the addition of the source term (Q_{SAS}) in the transport equation for the turbulence eddy frequency ω. In contrast, the equation for the turbulence kinetic energy k remains unchanged. The additional source term (Q_{SAS}) is given as:

$$Q_{SAS}=\max\left[\xi_2\kappa S^2\left(\frac{L}{L_{vK}}\right)^2 - C_{SAS}\frac{2\rho k}{\sigma_\Phi}\max\left(\frac{1}{\omega^2}\frac{\partial\omega}{\partial x_j}\frac{\partial\omega}{\partial x_j},\frac{1}{k^2}\frac{\partial k}{\partial x_j}\frac{\partial k}{\partial x_j}\right),0\right] \tag{6}$$

where the model parameters are given by $\xi_2=3.51$ $\sigma_\Phi=2/3$, $C_{SAS}=2$, κ is the von Karman constant. The turbulence length scale (L) is calculated as:

$$L=\frac{\sqrt{k}}{c_\mu^{0.25}\omega} \tag{7}$$

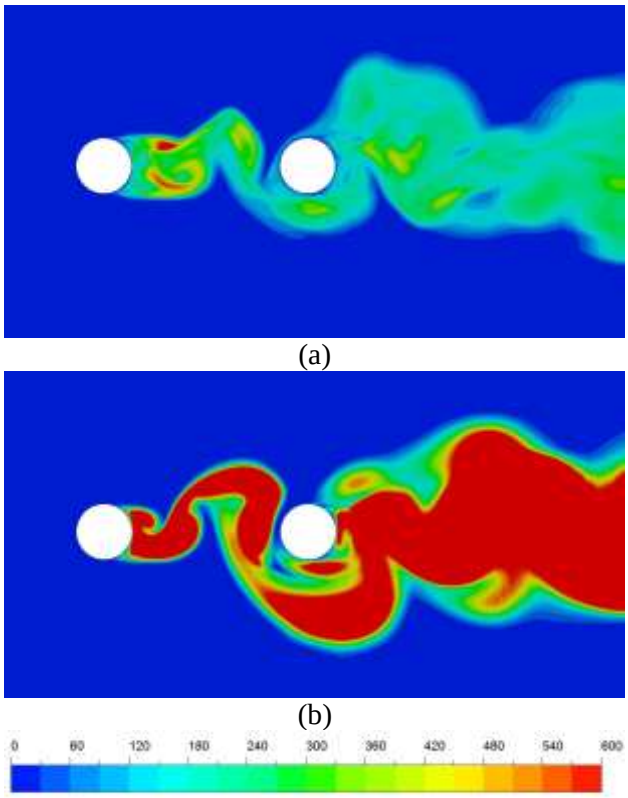

Fig. 1: Airflow past two circular cylinders arranged in tandem (Re = 1.66 x 10^5) - 2D contours snapshots of (υ_t/υ): a) SST-SAS turbulence model and b) k-ω SST turbulence model

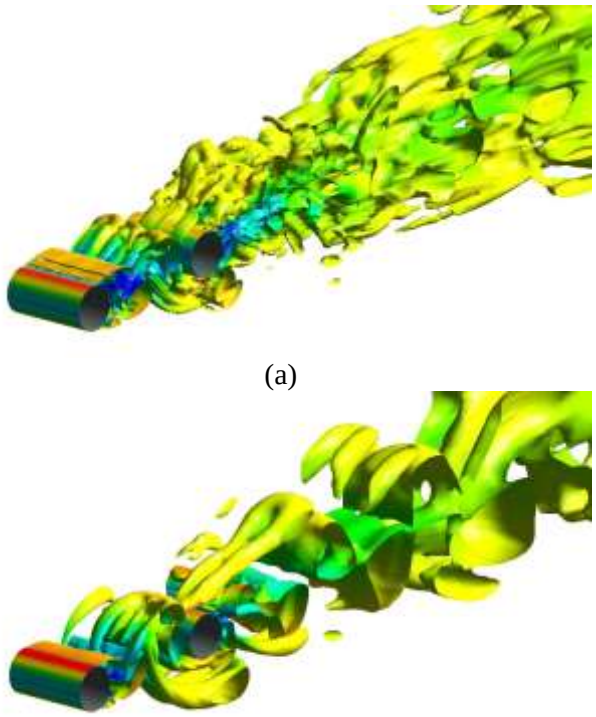

(a)

(b)

Fig. 2: Airflow past two circular cylinders arranged in tandem (Re = 1.66 x 10^5) - Snapshots of the Q-criterion iso-surface (Q = $1s^{-2}$) applied to the resolved velocity field: a) SST-SAS turbulence model and b) k-ω SST turbulence model

The von Karman length-scale L_{vK} acts as a sensor to detect the flow unsteadiness susceptibility of the resolved velocity field, which is defined as:

$$L_{vK} = \kappa \left| \frac{\dfrac{\partial \langle u_i \rangle}{\partial x_j}\dfrac{\partial \langle u_j \rangle}{\partial x_i}}{\left(\dfrac{\partial^2 \langle u_i \rangle}{\partial x_j^2}\right)\left(\dfrac{\partial^2 \langle u_j \rangle}{\partial x_i^2}\right)} \right|^{\frac{1}{2}} \tag{8}$$

In flow regions where Q_{SAS} is sufficiently large thanks to large values of $\left(\frac{L}{L_{vK}}\right)^2$, the turbulent viscosity $\upsilon_t \propto k/\omega$ experiences a dramatic reduction driven by the concomitant increase (resp. decrease) of ω (resp. k). This behavior is illustrated in Figure 1 for the flow past two cylinders in tandem at non-dimensional distance L/D = 3.7 (see section 3.2 for an in-depth analysis of such a flow configuration). It can be seen that when compared to the level obtained with a simulation based on the use of the sole k-ω model (Figure 1-(b)), an almost sixfold decrease in the maximum level of the turbulent eddy viscosity is obtained when using the SST-SAS model (Figure 1-(a)). The direct consequence of this reduction is the presence of a significantly broader range of structures in the cylinder's wakes when using the SST-SAS model. This phenomenon can be qualitatively illustrated by displaying representative iso-surfaces of the Q-criterion (Q = $1/2(\Omega^2$-$S^2)$, where S is the strain rate and Ω is the vorticity) obtained by processing two individual snapshots of the resolved flow fields. As depicted in Figure 2-(a), the presence of small-scale structures in the flow field is clearly visible in the snapshot of the resolved field obtained with the SST-SAS model whereas these small-scale structures are absent on the snapshot taken from the simulations with the standard k-ω SST turbulence model (Figure 2-(b)).

3 Case Analysis and Discussion

Despite the great simplicity of its geometry, the configuration obtained by uniformly flowing at a velocity U_∞ a fluid of kinematic viscosity υ past a circular cylinder of diameter D features quite a fascinating diversity of flow patterns and related dynamics as suggested by [31]. Since the beginning of the twentieth century, a great deal of studies focused on the characterization of the different flow regimes whose onset proved to be driven by the value of the Reynolds number defined as Re = $U_\infty D/\upsilon$. Still relevant today, the extensive review published in 1991 by [32] provided quite a complete panorama regarding the complexity of such a flow configuration. As recalled by [33], there exists three different flow regimes when progressively increasing Re: the subcritical regime ($Re \leq$ 1.5-2 x 10^5), the supercritical regime (4-5 x $10^5 \leq Re \leq$ 4-5 x 10^6) and the transcritical regime ($Re \geq$ 4-5 x 10^6. [32], split the subcritical regime into not less than seven different sub-regimes and thanks to visualizations they explained the different underlying and differentiating mechanisms that led to such a classification of the subcritical regime. The interested reader is referred to the review by, [32] and the references therein for further explanations regarding the mechanisms at work in this kind of flow configuration. If additional complexity comes into play such as with the presence of confinement, [34], or of additional cylinders, then what was observed for the isolated 1-cylinder flow configuration has to be revisited to account for new mechanisms of interference. This is precisely such kind of situations that call for

numerical simulations to help explain and predict the outcome of such complex interference. Along these lines, the objective of this section is to highlight the capability of numerical simulations (in particular with the SST-SAS turbulence model) to help investigate three different flow past cylinder(s) configurations characterized by the specific nature of the interference to be dealt with, namely: a circular cylinder in proximity to a plane wall, circular cylinders in a free stream arranged in tandem and the flow through a staggered tube bundle.

3.1 The Flow over a Circular Cylinder in the Vicinity of a Plane Wall

A notable feature of the flow past a circular cylinder in the subcritical regime is the unsteadiness of the cylinder wake. Taking the form of a periodic vortex shedding, it leads to the continuous application of fluctuating forces exerted on the cylinder. However, when the cylinder is positioned close to a plane wall at a distance of G, the flow dynamics become more complex. In such a configuration, distinct changes in aerodynamic drag and lift forces are observed. There exists a critical gap ratio ($(G/D)_{crit}$) for which the suppression of vortices takes place. This phenomenon is primarily controlled by three key parameters: the Reynolds number (Re), the boundary layer thickness (δ), and the gap ratio (G/D). Various computational fluid dynamics methods employed to investigate such a flow configuration are now discussed. Let's start with [35], who studied the conditions for observing the suppression of the vortex shedding for a Reynolds number Re ranging from 80 to 1000. They solved the 2D Navier–Stokes equations by using a finite difference method. Their results showed that the critical gap ratio ($(G/D)_{crit}$), at which the vortex shedding was suppressed was a decreasing function of the Reynolds number. [36], solved also the 2D Navier–Stokes equations but using a stream-function/vorticity formulation. For Re = 1200 and G/D = 0.5 and 1.5, they found the calculated lift and drag coefficients and the predicted vortex shedding behavior match well with available experimental results. [37], employed the 2D Unsteady Reynolds-Averaged Navier Stokes (URANS) equations with the standard high Reynolds number k–ε model at Re ranging from 1 x 10^4 to 4.8 x 10^4 with δ/D = 0.14-2. They reported an under-prediction of hydrodynamic quantities (C_d, C_l, St, and C_p) and attributed this to the intrinsic limitations of the k–ε model for such a flow configuration. In a subsequent study, [38], investigated near-bed flow mechanisms around a marine pipeline close to a flat seabed at Re = 3.6 x 10^6. The predicted hydrodynamic quantities were in satisfactory agreement with published experimental data. In their simulations at Re = 2 x 10^4, [39], selected the k-ω model. Their results exhibited good qualitative agreement with published experimental data. However, detailed comparisons with experimental results and discussions for G/D < 0.4 were not provided. [40], used both URANS and the Detached-Eddy Simulation (DES) to simulate the flow around a circular cylinder positioned near a moving plane wall at Re = 4 x 10^4. They found that DES proved superior to URANS in predicting the disappearance of vortex shedding as well as the time-averaged drag coefficients, the separation angles, and the velocity profiles in the near-wake region. The SST-SAS turbulence model was selected by [12], to conduct two-dimensional (2D) simulations around a circular cylinder positioned near a plane wall. The simulations considered factors such as wall proximity, boundary layer effects, and the variation of Reynolds number. Furthermore, three-dimensional (3D) simulations were also carried out to assess the importance of three-dimensional effects, [10]. Comparative analyses demonstrated a superior performance of the 3D simulations concerning the prediction of aerodynamic characteristics, and vortex shedding as well as the prediction of the critical values of ($(G/D)_{crit}$) at which the suppression of vortex shedding occurred. [41], shared a similar perspective, suggesting that 3D Large Eddy Simulation (LES) offers distinct advantages over the widely used 2D Reynolds-Averaged Navier-Stokes (RANS) k–ε model [42], as well as over 2D LES. The 3D LES results offer more reliable integrated forces and better capture flow details for different values of G/D. Additionally, in [11], the results obtained with the SST-SAS turbulence model showed that $(G/D)_{crit}$ decreased as Re was increased from 8.6 x 10^4 to 2.77 x 10^5, a trend similar to that observed by [38]. However, in [10], the change in $(G/D)_{crit}$ was associated more with the shift in flow regimes (from subcritical to critical) than with a change in the Reynolds number itself. On the other hand, the critical gap was not overly sensitive to the incident boundary layer thickness (δ) since for Re = 1.89 x 10^5, the results showed that $(G/D)_{crit}$ decreased from 0.3 to 0.2 when δ/D was increased from 0.1 to 1.1. This trend was echoing the findings by [43] and [44].

3.2 Circular Cylinders Arranged in Tandem in a Free Stream

Placing more than one cylinder within the fluid stream leads to the so-called flow interference

regime. The tandem configuration corresponds to the case of two cylinders arranged in line in a crossflow. The wake of the upstream cylinder modifies the incoming flow conditions for the downstream cylinder, while this second cylinder interferes with the wake dynamics and vortex formation region of the upstream cylinder. [45], described this reciprocal impact as 'wake interference'. Depending on the distance between the cylinders, different flow behaviors occur around both cylinders that have significant effects on the vortice detachment and the resulting loads on the cylinders. The distance between the cylinders called the spacing is expressed as the ratio of the center-to-center distance L to the cylinder diameter, denoted as L/D. Particularly crucial is the critical spacing $(L/D)_{crit}$ associated with the onset of the vortex shedding from the upstream cylinder.

Many computational studies of tandem cylinders in steady cross-flow have been undertaken. [46], used a fractional step method at Re varying from 100 to 200 to analyze the flow around multiple cylinders. The numerical simulation approach has been less effective compared to the experimental data, due to the intricacy of the flow across cylinders, [47]. [48], considered a laminar flow regime at Re = 100 for a six-row inline tube bank. A critical spacing range between 3.0 and 3.6 was identified at which the mean drag as well as the RMS (root mean square) lift and drag coefficients for the last three cylinders reached their maximum values. In [49], a standard LES with the Smagorinsky subgrid-scale model was retained to explore the characteristics of the vortices shed from the circular tandem cylinders at $Re = 2.2 \times 10^4$ and L/D varying from 2 to 5. They found that the critical spacing was about L/D = 3.25 and the mean drag and fluctuating lift coefficients of each cylinder jumped to higher values for this critical spacing. [50], discussed the flow characteristics across tandem circular cylinders in the range of subcritical ($Re = 2.4 \times 10^4$) and supercritical ($Re = 3.0 \times 10^6$) regimes by numerical simulation at L/D ranging from 2 to 5 by means of improved delayed DES (IDDES) method. They demonstrated that for both Reynolds numbers, the vortex shedding occurred from both upstream and downstream cylinders as soon as $L/D \geq 3.5$. Moreover, the fluctuating lift coefficients of the upstream cylinder were almost independent of Re, but those of the downstream cylinder dropped as Re was increased. In [51], Delayed Detached Eddy Simulations (DDES) were used to simulate the flow around tandem circular cylinders at L/D = 3.7 and $Re = 1.66 \times 10^5$. Simulations were performed on a (relatively) coarse grid containing about 31 million grid points, and on a fine grid containing about 133 million grid points. The conclusion drawn was that some of the fine grid DDES results were not significantly different from those obtained with the coarse grid DDES. [52], simulated the flow interference between tandem cylinders based on the hybrid RANS/LES methods with non-linear eddy viscosity formulations at $Re = 1.66 \times 10^5$ for L/D = 1.4, 3, and 3.7. The presence of a bistable wake between the cylinders and the subsequent drag inversion on the downstream cylinder was noted at L/D = 3. Additionally, it was observed that the bistable wake resulted in an elevation of the turbulent kinetic energy level within the gap between the cylinders.

The evaluation of the SST-SAS model's performance was conducted in the analysis of the flow around two circular cylinders of identical diameter arranged in tandem at a high subcritical Reynolds number ($Re = 1.2 \times 10^5$) by [13]. Additionally, [53], employed a numerical model that combines Reynolds-Averaged Navier-Stokes (RANS) and Large Eddy Simulation (LES) to simulate the flow around two tandem cylinders at $Re = 1.66 \times 10^5$ for L/D = 3.7. In this study, the results obtained with the SST-SAS model were utilized only for comparative purposes. In [13], interference effects for distances L/D varying from 1.1 to 7 were explored by comparing them with those obtained for the flow around a single isolated cylinder. The results under-predicted the mean drag coefficient for the upstream cylinder, while that for the downstream cylinder provided they were in satisfactory agreement with their experimentally obtained counterparts. A critical spacing value of $(L/D)_{crit} = 3$ and the flow patterns associated with the bistable flow, [54], were also observed.

3.3 Staggered Tube Bundle

The flow through bundles of cylinders has been mostly investigated in the context of heat exchanger design and analysis. This configuration exhibits a vortex shedding behavior quite similar to that observed for the flow past a single cylinder but with the added complexity of strong interactions between the wakes of the tubes. This configuration represents quite a challenging test case for any existing model or newly derived model. Indeed, many researchers have simulated this configuration using a broad range of approaches, from RANS models to Direct Numerical Simulation (DNS). For validation purposes, many of these studies used the experimental data obtained in [55], [56], [57], for the configuration of water flowing through a staggered tube bundle array at Re = 18000.

[58], examined the turbulent flow through a tube bundle at a Reynolds number of 9300, both experimentally and numerically. They closed the steady RANS equations by using four different turbulence models: k–ε, k–ω, SST, and the Reynold Stress Model (RSM). The Reynolds normal stresses approximated from the k–ω and SST models demonstrated a closer agreement with experiments than those obtained from the RSM model. However, these RANS simulations failed to provide reliable predictions for this flow due to the poor estimation of the turbulence kinetic energy behavior. [59], applied RANS and URANS simulations to predict the experiments in [55], [56], [57]. URANS simulations using a Reynolds stress model (RSM) exhibited better agreement with experimental data than the 2-equation model, although some discrepancies persisted, particularly when it came to reproducing the Reynolds normal stress behavior. [60] and [61], investigated the same flow configuration as [59], and reached similar conclusions when comparing the results of RANS and URANS simulations. [62], employed LES and a k–ε model to simulate experiments configuration in [55], [56], [57]. They reported well-predicted mean velocity profiles in both cases. However, in the wake region, the k–ε model provided a poorer quality of prediction of the Reynolds stresses compared to LES. [63], utilized LES, coarse LES, and RSM-based URANS approaches to model the flow in [55], [56], [57], at a Reynolds number of 9000. They reported that both the LES and RSM-based URANS approach provided satisfactory results compared to experiments, with the former being slightly more consistent with DNS results. A study by [64], employed Partially Filtered Navier–Stokes (PANS) and LES, reporting that both methods predicted the flow with relatively good agreement with experimental data, although PANS simulation was conducted on a much coarser grid than LES. [65], used 3D DNS to predict experiments in [55], [56], [57], at a lower Reynolds number (Re = 6000) to limit the computational cost. The results were in good agreement with the experiments. Additionally, [66], performed DNS simulations of the flow through a staggered tube bundle over the range $1030 \leq Re \leq 5572$. One of their objectives was to determine the Reynolds number value at which transition occurs at the matrix transition point e.g. the point at which the second frequency peak becomes prominent in the spectral signature of the vortex shedding. They observed that such a transition occurred at $Re \approx 3000$, a value similar to that observed for the transition for the single-cylinder flow configuration.

The study by [18], delved into the predictive capabilities of the SST-SAS turbulence model. They simulated the flow configuration in [55], [56], [57]. Their results proved to be quite satisfactory when compared with the experimental data in terms of both mean velocity components and turbulence quantities. The study introduced a quantitative objective scoring criterion, utilizing relevant norms to compare the SST-SAS results with those obtained from other models in the literature. The comparison revealed that the SST-SAS model presented a remarkable consistency in its predictive capability, ranking among the top-performing models in agreement with experimental data. Moreover, in [18], an in-depth analysis of the Reynolds stress tensor's behavior was conducted for unsteady URANS models. The analysis utilized the triple decomposition of the instantaneous velocity field. The findings indicated that, in the case of the SST-SAS model, the contribution of time-resolved motion to the total velocity correlations was significantly higher when compared to other URANS models, reaching levels exceeding 95 %.

4 Wall-mounted Cylinder

"The more available experimental data, the better for simulation validation" is the motto behind the choice of building up a new experiment on turbulent flows over a wall-mounted cylinder to create a database that will be subsequently made available in open access. The configuration represents a distinctive case where the cylinder encounters the flow passage from only one side. The experimental and numerical results reported here are restricted to a low Reynolds subcritical flow at Re = 2300 based on the diameter of the cylinder D = 0.04 m, the kinematic viscosity of air $\upsilon = 1.53 \times 10^{-5}\ m^2/s$, and the bulk velocity $U_{bulk} = 0.88\ m/s$.

4.1 Experimental Set-Up and Metrology

The MAVERIC test facility installed on the premises of LMAP (CNRS/Pau University, France) for studying effusion cooling flows, [67], [68], was updated to accommodate a specifically designed test section housing a removable cylinder of the circular cross-section. A side view of the test section fitted with the cylinder is displayed in Figure 3. The rig consists basically of two 2.5 m-long superimposed separate channels of identical rectangular cross-section (width W = 400 mm x height H = 120 mm) followed by the Plexiglas-made test section. Each channel is fed in air by a dedicated centrifugal fan powered by a 1-KW electrical motor regulated in

rotation by a Siemens Micro-Master MC420 controller. The test section which accommodates the plate supporting the removable cylinder in the upper channel is followed by the exhaust section which evacuates outside the airflow through the lateral wall of the laboratory. A two-component planar particle image velocimetry (PIV) LaVision system combined with computer-controlled translation stages permitted to selection the desired image plane by accurately displacing the Imager Pro X CCD recording camera (1600 pixels *x* 1200 pixels, intensity range over 14 bits, 50 *mm* lens, f-number = 4). The airflow was seeded with Di-Ethyl-Hexyl-Sebacat (DEHS) particles of 1 μm of average diameter. A double-pulse Nd-Yag laser combined with divergent optics produced a divergent laser sheet (wavelength = 532 *nm*, thickness of the sheet ≈ 1 *mm*) introduced normally in the flow through the top wall of the test section (Figure 3).

All the measurements were made in the mid-plane of the channel. Twelve hundred double-frame recordings featuring a 10-*pixel/mm* resolution were acquired for three different streamwise positions of the camera to cover a flow region extending from 6 *D* upstream to 6 *D* downstream of the cylinder. The number of recordings was chosen to ensure the convergence of the estimator of the average of the two velocity components. The recordings were first pre-processed by i) subtracting the background images obtained by firing the lasers without seeding the flow and ii) normalizing the particle intensity. Then, these pre-processed recordings were successively processed by a multi-pass cross-correlation algorithm (LaVision Davis Software 8.4.0) using interrogation windows of decreasing size from 96 pixels *x* 96 pixels down to 32 pixels *x* 32 pixels.

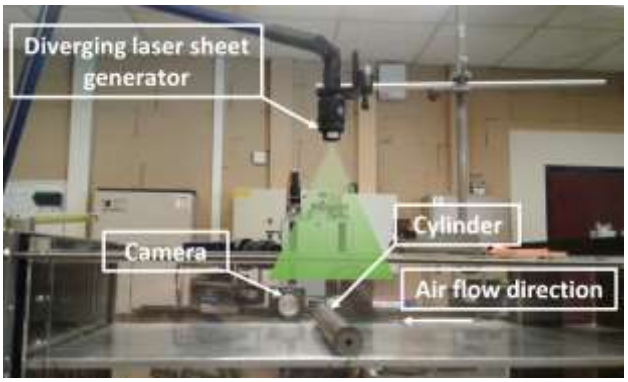

Fig. 3: Wall-mounted cylinder - Side view of the test section of the MAVERIC rig and some components of the PIV system

4.2 Numerical Set-Up

The numerical solver used in this research was the commercial CFD code Ansys Fluent 15, in line with [69]. This code employs the finite volume cell-centered method to solve the governing equations describing fluid motion in a segregated manner. Spatial discretization of these equations was performed on three-dimensional structured grids generated with ICEM CFD. Convection terms were discretized using a bounded central differencing scheme, while pressure and turbulent quantities (k and ω) were evaluated with a second-order scheme. Further, the equations were discretized in time using a bounded second-order implicit scheme. The pressure-velocity coupling was managed using the SIMPLE (Semi-Implicit Method for Pressure-linked Linked Equations) algorithm, [70]. Results from [71], utilizing the SST-SAS turbulence model demonstrated that SIMPLE exhibits acceptable performances in resolving unsteady turbulent flow around a circular cylinder, requiring less computational time compared to the SIMPLEC [72] and PISO [73] approaches.

4.2.1 Boundary Condition

Figure 4 depicts a schematic of the computational domain and of the boundary conditions employed. Inlet conditions for this investigation are established using a velocity profile outlined in Eq. (9). The resulting profile is incorporated as an input condition through the User-Defined Function (UDF) provided by the code. At the outlet, a reference zero pressure condition is applied. For the upper and lower limits of the domain, a no-slip wall condition is specified. The same condition of zero velocity on the wall is applied to the surface of the cylinder. Lastly, at the lateral limits (normal to the $x-y$ plane), periodicity conditions are imposed, considering that we are dealing with a reduced 2D model corresponding to the length of the cylinder.

$$U_{(y)} = \begin{cases} if\ y < 0.052 & U_{bulk}\left(\frac{y}{0.06}\right)^{0.2} \\ if\ 0.052 \le y \le 0.068 & 0.98U_{bulk} \\ if\ y > 0.068 & U_{bulk}\left(\frac{0.12-y}{0.06}\right)^{0.13} \end{cases} \quad (9)$$

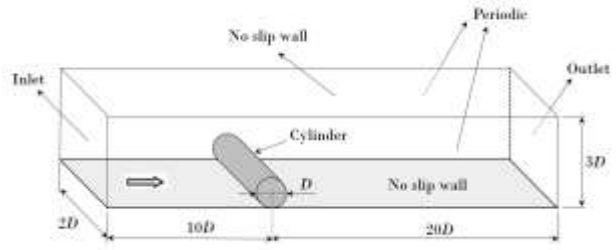

Fig. 4: Flow around a wall-mounted circular cylinder at *Re* = 2300 - Schematic of the computational domain and boundary conditions used for the simulations. The diameter of the cylinder is *D* = 40 *mm*

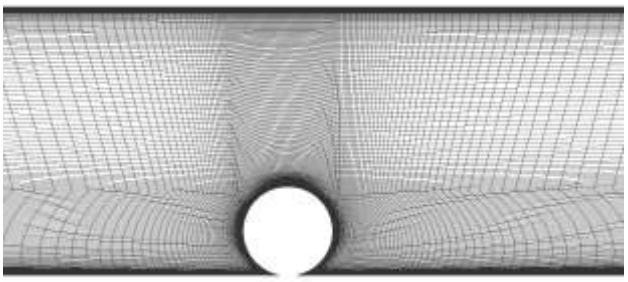

(a)

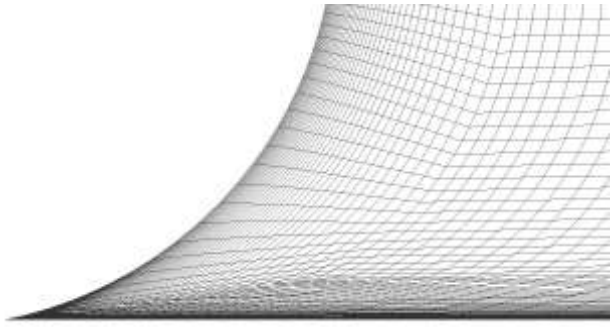

(b)

Fig. 5: Flow around a wall-mounted circular cylinder at *Re* = 2300 - 2D cutting view of the 3D structured mesh: a) Overview of the mesh and b) Detail at the intersection between the supporting wall and the cylinder surface

4.2.2 Mesh

The three-dimensional mesh is generated by extending the two-dimensional mesh (Figure 5) in the *z* direction, spanning it over a distance equal to twice the cylinder diameter. Figure 5-(a) provides an overall view of the mesh which featured refinement near the cylinder surface and at the level of the upper and lower limits of the domain. This refinement was crucial for accurately capturing the boundary layer on these surfaces, ensuring that the normal distance to the wall of any wall-adjacent cell satisfied $y^+ < 1$. Figure 5-(b) illustrates how the structured mesh was adapted to reproduce accurately the acute angle formed between the bottom of the cylinder and the supporting wall.

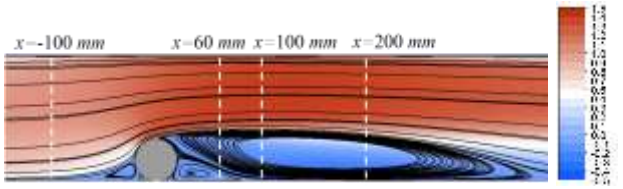

(a)

(b)

(c)

(d)

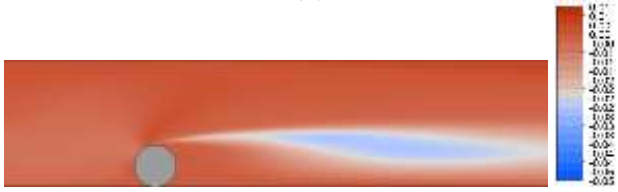

(e)

Fig. 6: Flow around a wall-mounted circular cylinder at *Re* = 2300 - Contours of the velocity field (*m/s*) and average Reynolds stress fields (m^2/s^2); (a) streamwise component of the velocity; (b) normal component of the velocity; (c) longitudinal Reynolds stress *Rxx*; (d) normal Reynolds stress *Ryy*; (e) shear Reynolds stress *Rxy*

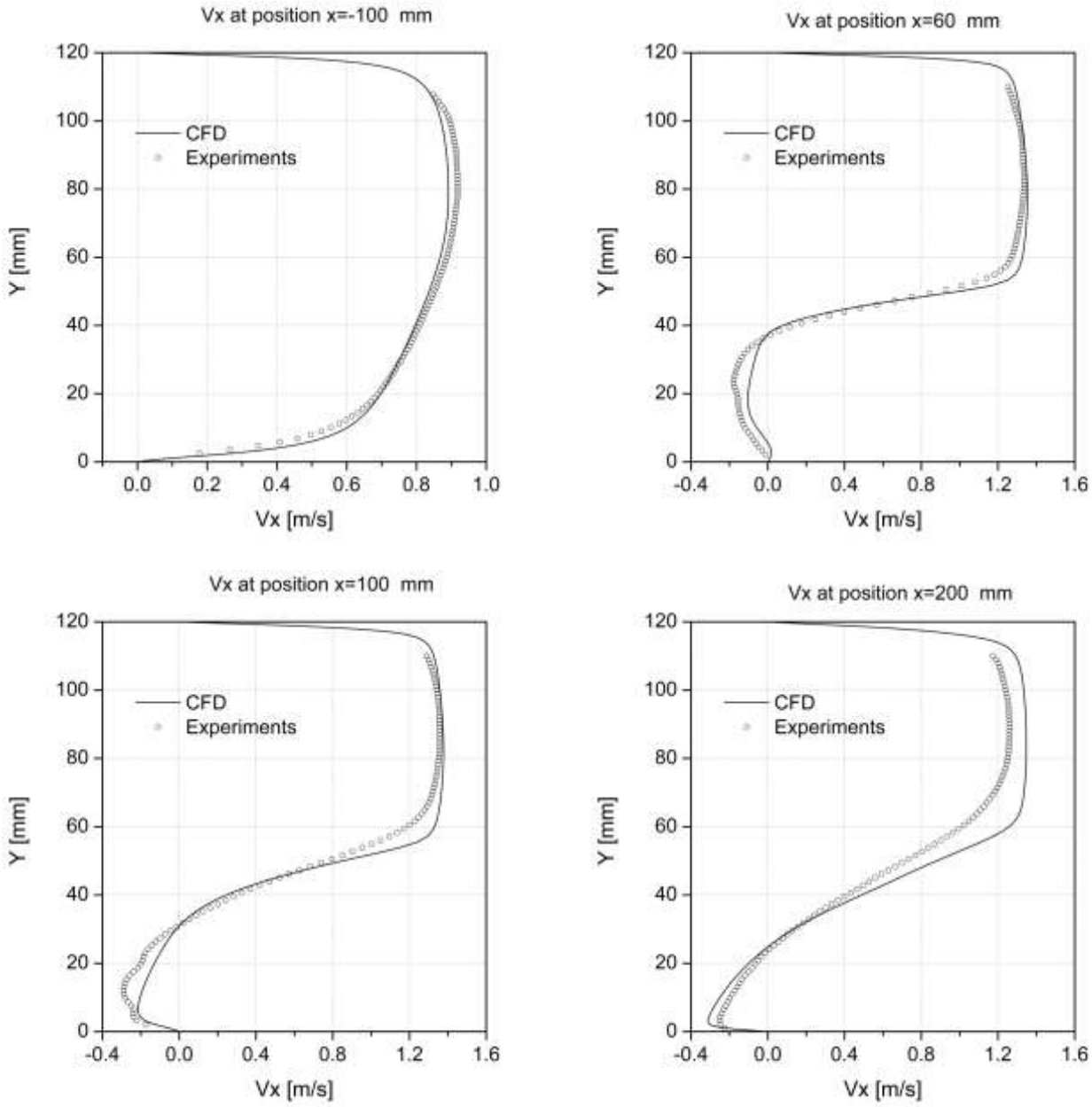

Fig. 7: Flow around a wall-mounted circular cylinder at *Re* = 2300. Profiles of the time average of the streamwise velocity component at four vertical cross-sections. Upper left: upstream position at *x* = -100 *mm* (*x/D* = -2.5). Upper right: downstream position at *x*=60 *mm* (*x/D* = 1.5). Lower left: downstream position at *x* = 100 *mm* (*x/D* = 2.5). Lower right: downstream position at *x* = 200 *mm* (*x/D* = 5)

4.3 Illustration of the Average Flow Field

The simulated flow field is initially illustrated by presenting the time average of the fields of the two velocity components, Vx (Figure 6-(a)) and Vy (Figure 6-(b)), along with the fields of three components of the Reynolds stress tensor (Figure 6-(c) to 6-(d)).

In both time averages of the resolved fields of Vx and Vy, a small recirculation zone can be observed e.g. where the streamlines approaching the cylinder appear to bifurcate. One part of the flow is directed towards the upper surface of the cylinder, while the other part is oriented towards the wall, hence delimitating a recirculation zone. The flow bifurcation point and the recirculation zone closely resemble those obtained by PIV for a cylinder in contact with a plane wall at *Re* = 3000 by [74] (refer to Figure 2 in their study). It is worth stressing that in [74], was visualized the flow only in the region in front of and above the cylinder, making a direct comparison challenging for the recirculation region generated behind the cylinder. Nevertheless, a comparison is feasible for the region behind the cylinder with the PIV data obtained by [75], at *Re* =

5000. Although the Reynolds number is slightly different, it's apparent that the main recirculation and the recirculation generated just behind the cylinder and the lower limit (Figure 6-(a) and (b)) are highly similar to those obtained for *Re* = 5000 (Figure 2 in [75]).

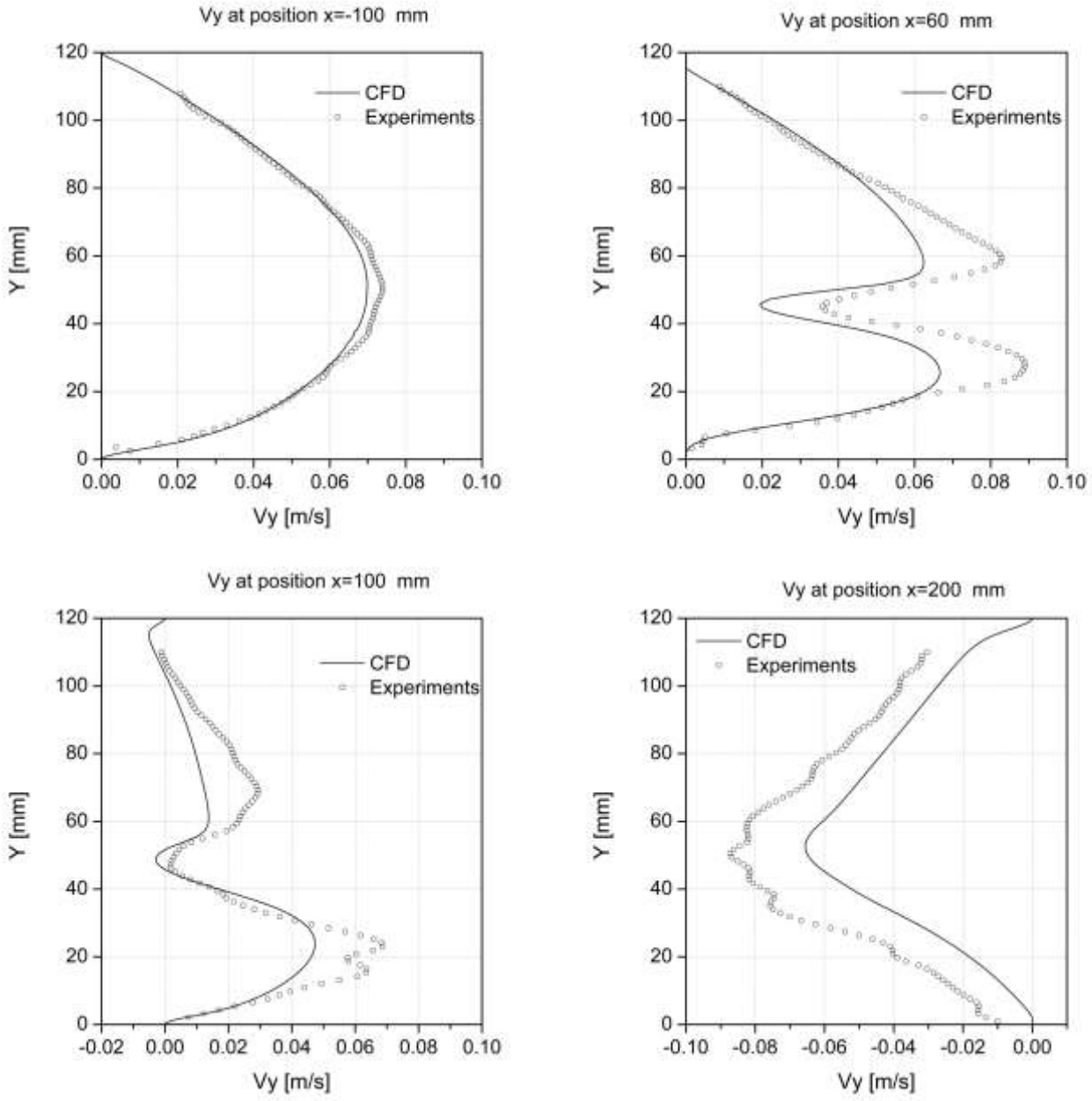

Fig. 8: Flow around a wall-mounted circular cylinder at *Re* = 2300. Profiles of the time average of the normal velocity component at four vertical cross-sections. Upper left: upstream position at *x* = -100 *mm* (*x/D* = -2.5). Upper right: downstream position at *x*=60 *mm* (*x/D* = 1.5). Lower left: downstream position at *x* = 100 *mm* (*x/D* = 2.5). Lower right: downstream position at *x* = 200 *mm* (*x/D* = 5)

4.4 Preliminary Comparison of PIV vs CFD Results

The normal profiles of the streamwise and the normal components of the velocity and their experimentally obtained counterparts are shown in Figure 7 and Figure 8 at four different abscissas. The corresponding vertical cross-sections are materialized by vertical dashed cutting lines in Figure 6-(a) and (b). The prediction of the velocity component profiles with SST-SAS proved to be quite satisfactory when compared to their experimental counterpart. Indeed, the profiles of the velocity streamwise component (Vx) are very well predicted by the SST-SAS calculations for the three positions at x = 60, 100, and 200 *mm* which represent the recirculation zone downstream of the cylinder. Regarding the normal velocity component Vy, the comparison is qualitatively good but features some significant discrepancies indicating that the predicted and the measured recirculation zones might have slightly different dimensions. The use of the triple decomposition of the instantaneous velocity field, [18], showed that the contribution of the resolved part of the motion to the total Reynolds stress was negligible. In simpler terms, the velocity unsteadiness is dampened, resulting in a fully steady state for the flow. Consequently, for this flow configuration, the Q_{SAS} term does not play a determinant role as observed in the preceding cases indicating that the standard k-ω SST model is recovered in this case.

5 Conclusion

This review strongly supports the notion that the SST-SAS model is a highly relevant choice for simulating unsteady flows around bluff bodies. From both a qualitative and quantitative points of view, the predictive capacity of SST-SAS based simulations proved to be quite superior to those provided by standard RANS models and to match at quite an affordable cost those obtained by the most advanced simulation tools such as the family of LES based approaches. However the world of turbulence modeling is far from being frozen as new "competitors" are continuously emerging. This is the case of the so-called hybrid temporal LES (HTLES) advocated by Manceau and his group [76], [77]. In its version based on the SST-SAS model on a modification of the k-ω SST model, the HTLES provides quite a sound alternative to the SST-SAS approach. Comparing the performances of both approaches will be one of the topics of our future activity as well as the enrichment and publication of the PIV database for the configuration of the flow past wall-mounted cylinder(s).

Acknowledgement:
The authors express their gratitude to the National University of Córdoba, the National University of Cuyo, and the University Pau & Pays Adour for their valuable support. Additionally, the first author acknowledges the support of CONICET in sustaining this research. This work is dedicated to the memory of Ph.D. Jose Tamagno, is a distinguished expert in fluid mechanics whose legacy continues to influence our understanding of this field.

References:

[1] Hanjalic, K., Launder, B., Eddy-Viscosity transport modelling: A historical review, *in: 50 Years of CFD in Engineering Sciences*, Springer, pp. 295-316, 2020.

[2] Al-Khalidy, N., Building Generated Wind Shear and Turbulence Prediction Utilising Computational Fluid Dynamics, *WSEAS Transactions on Fluid Mechanics*, Vol.13, pp. 126-135, 2018.

[3] Menter, F.R., Egorov, Y., A Scale Adaptive Simulation model using two-equation models. *AIAA Paper 2005*, Vol. 1905, pp. 1-13, 2005.

[4] Egorov, Y., Menter, F., Development and application of SST-SAS turbulence model in the DESIDER project. *Notes on Numerical Fluid Mechanics and Multidisciplinary Design*, Vol.97, pp. 261–270, 2008.

[5] Menter, F.R., Two-equation eddy-viscosity turbulence models for engineering applications. *AIAA Journal*, Vol.32, pp. 1598–1605, 1994.

[6] Shahi, M., Kok, J.B.W., Pozarlik, A., On characteristics of a non-reacting and a reacting turbulent flow over a backwards facing step (BFS). *International Communications in Heat and Mass Transfer*, Vol.61, pp. 16-25, 2015.

[7] Hundshagen, M., Casimir, N., Pesch, A., Falsafi, S., Skoda, R., Assessment of scale-adaptive turbulence models for volume-type centrifugal pumps at part load operation. *International Journal of Heat and Fluid Flow*, Vol. 85, 108621, 2020.

[8] Menter, F., Elements, and applications of Scale-Resolving Simulation methods in industrial CFD. *Fröhlich, J., Kuerten, H., Geurts, B., Armenio, V. (Eds.), Direct and Large-Eddy Simulation IX, ERCOFTAC*

Series, Vol. 20, Springer, Cham, pp. 179-195, 2015.

[9] Zheng, W., Yan, C., Liu, H., Luo, D., Comparative assessment of SAS and DES turbulence modeling for massively separated flows. *Acta Mechanica Sinica*, Vol.32, pp. 12 21, 2016.

[10] Grioni, M., Elaskar, S., Mirasso, A., Scale-Adaptive Simulation of flow around a circular cylinder near a plane boundary. *Journal of Applied Fluid Mechanics*, Vol.11, No.6, pp. 1477-1488, 2018.

[11] ElCheikh, A., ElKhoury, M., Effect of local grid refinement on performance of scale-resolving models for simulation of complex external flows. Aerospace, Vol.6, No.8, 2019.

[12] Grioni, M., Elaskar, S., Mirasso, A., Numerical simulation of flow around circular cylinder near a plane wall: effects of wall proximity, boundary layer and Reynolds number. *South Florida Journal of Development*, Vol.4, No.5, pp. 2099-2113, 2023.

[13] Grioni, M., Elaskar, S., Mirasso, A., A numerical study of the flow interference between two circular cylinders in tandem by Scale-Adaptive Simulation model. *Journal of Applied Fluid Mechanics*, Vol.13, No.1, pp. 169-183, 2020.

[14] Duan, Y., Cooling, C., Ahn, J.S., Jackson, C., Flint, A., Eaton, M.D., Bluck, M.J., Using a Gaussian process regression inspired method to measure agreement between experiment and CFD simulations. International Journal of Heat and Fluid Flow, Vol.80, 108497, 2019.

[15] Taghinia, J., Rahman Mizanur, M., Siikonen, T., Numerical investigation of twin-jet impingement with hybrid-type turbulence modeling. *Applied Thermal Engineering*, Vol.73, pp. 650-659, 2014.

[16] Munoz Paniagua, J., García, J., Lehugueur, B., Evaluation of RANS, SAS and IDDES models for the simulation of the flow around a high-speed train subjected to crosswind. *Journal of Wind Engineering and Industrial Aerodynamics*, Vol. 171, pp. 50-66, 2017.

[17] Niu, X.-F., Li, Y., Wang, X.-N, Numerical study of aerodynamic noise behaviors for a vertically installed flat strut behind an asymmetrical airfoil. European Journal of Mechanics / B Fluids, Vol.88, pp. 17-33, 2021.

[18] Grioni, M., Bruel, P., Elaskar, S., Mirasso, A., An application of the scale adapted simulation to the unsteady flow across a tube bundle. *International Journal of Heat and Fluid Flow*, Vol.96, pp. 109007, 2022.

[19] Zhao, H., gao, P., Tian, R., Li, X., A three-dimensional refined numerical simulation of cross-flow induced vibration mechanism in the tube bundle. *Nuclear Engineering and Design*, Vol.405, 112223, 2023.

[20] Si, Q., Yuan, J., Yuan, S., Wang, W., Zhu, L., Bois, G., Numerical investigation of pressure fluctuation in centrifugal pump volute based on SAS model and experimental validation. *Advances in Mechanical Engineering*, Vol. 2014, P72081, 2014.

[21] Kurec, K., Piechna, J., Gumowski, K., Investigations on unsteady flow within a stationary passage of a pressure wave exchanger, by means of PIV and CFD calculations. *Applied Thermal Engineering*, Vol. 112, pp. 610-620, 2017.

[22] Gonin, R., Horgue, P., Guibert, R., Fabre, D., Bourguet, R., Ammouri, F., Vyazmina, E., Advanced modeling improves thermal thermal gradient prediction during compressed hydrogen tank filling. *International Journal of Hydrogen Energy*, Vol. 48, pp. 30057-30068, 2023.

[23] Shukla, S., Singh, S.N., Sinha, S.S., Vijayakumar, R., Comparative assessment of URANS, SAS and DES turbulence modeling in the predictions of massively separated ship air wake characteristics. *Ocean Engineering*, Vol. 229, 108954, 2021.

[24] Sotoudeh, N., Maddahian, R., Cervantes M.J., Investigation of a rotating vortex rope formation during load variation in a Francis turbine draft tube. *Renewable Energy*, Vol.151, pp. 238-254, 2020.

[25] Salehi, S., Nilsson, H., Lillberg, E., Edh, N., An in-depth numerical analysis of transient flow field in a Francis turbine during shutdown. *Renewable Energy*, Vol. 179, pp. 2322-2347, 2021.

[26] Arabnejad, M.H., Nilsson, H., Bensow, R.E., Investigation of flow-induced instabilities in a Francis turbine operating in con-cavitating and cavitating part-load conditions. *Fluids*, Vol.8, No.2, 61, 2023.

[27] Menter, F., Kuntz, M., Bender, R., A Scale-Adaptive Simulation model for turbulent flow predictions. *AIAA Paper 2003*, Vol.0767, pp. 1-11, 2003.

[28] Menter, F., Egorov, Y., Revisiting the turbulent scale equation, *in IUTAM Symposium on One Hundred Years of*

Boundary Layer Research, Springer, Vol.129, 2006.

[29] Menter, F., Egorov, Y., The Scale-Adaptive Simulation method for unsteady turbulent flow predictions. part 1: theory and model description. *Flow, Turbulence and Combustion*, Vol.85, No.1, pp. 113-138, 2010.

[30] Davidson, L., Evaluation of the SST-SAS model: channel flow, asymmetric diffuser, and axi-symmetric hill. *in: Proc. of ECCOMAS 2006, Egmond aan Zee, Netherlands*, pp. 1-20, 2006.

[31] Morkovin, M.V., Flow around circular cylinder−a kaleidoscope of challenging fluid phenomena. In Proceedings of the ASME Symposium on Fully Separated Flows, *ASME, New York*, pp. 102-118. 1964.

[32] Coutanceau, M., Defaye, Circular cylinder wake configurations: a flow visualization survey. *Applied Mechanics Reviews*, Vol.44, No.6, pp. 255-305, 1991.

[33] Farell, C., Blessmann, J., On critical flow around smooth circular cylinders. *Journal of Fluid Mechanics.* Vol.36, pp.375-391, 1983.

[34] Nguyen, Q.D., Lu, W., Chan, L., Ooi, A., Lei, C., A state-of-the-art review of flows past confined circular cylinders. *Physics of Fluids*, Vol.35, 071301, 2023.

[35] Lei, C., Cheng, L., Armfield, S.W., Kavanagh, K., Vortex shedding suppression for flow over a circular cylinder near a plane boundary. *Ocean Engineering*. Vol.27, pp. 1109-1127, 2000.

[36] Dipankar, A. and Sengupta, T. K, Flow past a circular cylinder in the vicinity of a plane wall. *Journal of Fluids and Structures*. Vol.20, pp. 403- 423, 2005.

[37] Ong, M.C., Utnes, T., Holmedal, L.E., Myrhaug, D., Pettersen, B., Numerical simulation of flow around a marine pipeline close to the seabed. *Coastal Engineering*. Vol.3, pp. 2730-2742, 2008.

[38] Ong, M.C., Utnes, T., Holmedal, L.E., Myrhaug, D., Pettersen, B., Numerical simulation of flow around a circular cylinder close to a flat seabed at high Reynolds numbers using a $k-\epsilon$ model. *Coastal Engineering*. Vol.57, pp. 931-947, 2010.

[39] Zhao, M., Cheng, L., and Teng, B., Numerical Modeling of Flow and Hydrodynamic Forces Around a Piggyback Pipeline Near the Seabed. Journal of Waterway, Port, *Coastal, Ocean Engineering*. Vol.133, No.4, pp. 286-295, 2007.

[40] Nishino, T., Roberts, G.T. and Zhang, X., Unsteady RANS and detached-eddy simulations of flow around a circular cylinder in ground effect. *Journal of Fluids and Structures*. Vol.24, pp. 18-33, 2008.

[41] Abrahamsen Prsic, M., Chen Ong, M., Pettersen, B., Myrhaug, D., Large Eddy Simulations of flow around a circular cylinder close to a flat seabed. *Marine Structures*. Vol.46, pp. 127-148, 2016.

[42] Ong, M.C., Utnes, T., Holmedal, L.E., Myrhaug, D., Pettersen, B., Near-bed flow mechanisms around a circular marine pipeline close to a flat seabed in the subcritical flow regime using a $k-\epsilon$ model. *Offshore Mech Arct Eng*. Vol.134, No.2, pp. 021803, 2012.

[43] Buresti, G. and Lanciotti, A., Mean and fluctuating forces on a circular cylinder in cross-flow near a plane surface. *Journal of Wind Engineering and Industrial Aerodynamics*. Vol.41, pp. 639-650, 1992.

[44] Lei, C., Cheng, L., Kavanagh, K, Reexamination of the effect of a plane boundary on force and vortex shedding of a circular cylinder. *Journal of Wind Engineering and Industrial Aerodynamics*. Vol.81, pp. 263-286, 1999.

[45] Zdravkovich, M., The effects of interference between circular cylinders in cross flow. *Journal of fluids and structures*. Vol.1, No.2, pp. 239-261, 1987.

[46] Meneghini, J.R., Saltara, F., Siqueira, C., Ferrari, J.Jr., Numerical simulation of flow interference between two circular cylinders in tandem and side-by-side arrangements. *Journal of fluids and structures*. Vol.15, No.2, pp. 327-350, 2001.

[47] Sumner D., Two circular cylinders in cross flow: a review. *Journal of fluids and structures*. Vol.26, pp. 849-899, 2010.

[48] Liang, C., Papadakis, G., Luo, X., Effect of tube spacing on the vortex shedding characteristics of laminar flow past an inline tube array: a numerical study. *Computers & Fluids*. Vol.38, No.4, pp. 950-964, 2009.

[49] Kitagawa, T. Ohta, H., Numerical investigation on flow around circular cylinders in tandem arrangement at a subcritical Reynolds number. *Journal of Fluids and Structures*. Vol.24, No.5, pp. 680-699, 2017.

[50] Hu X, Zhang X, You Y., On the flow around two circular cylinders in tandem arrangement at high Reynolds numbers. *Ocean Engineering*. Vol.189, pp. 106301, 2019.

[51] Uzun, A., Yousuff Hussaini, M., An application of delayed detached eddy simulation to tandem cylinder flow field prediction. *Computers & Fluids*. Vol.60, pp. 71-85, 2012.

[52] Gopalan, H., Jaiman, R., Numerical study of the flow interference between tandem cylinders employing non-linear hybrid URANS–LES methods. *Journal of Wind Engineering and Industrial Aerodynamics*. Vol.142, pp. 111-129, 2015.

[53] Weinmann, M., Sandberg, R., Doolan, C., Tandem cylinder flow and noise predictions using a hybrid RANS/LES approach. *International Journal of Heat and Fluid Flow*. Vol.50, pp. 263-278, 2014.

[54] Igarashi, T., Characteristics of the flow around two circular cylinders arranged in tandem: 1st report. *Bulletin of JSME*. Vol.24, No.188, pp. 232-331, 1981.

[55] Simonin, O., Barcouda, M., Measurements of fully developed turbulent flow across tube bundle. *in: Proceedings of the Third International Symposium on Applications of Laser Anemometry to Fluid Mechanics, Lisbon, Portugal*, 1986.

[56] Simonin, O., Barcouda, M., Measurements and prediction of turbulent flow entering a staggered tube bundle. *in: Proceedings of the Fourth International Symposium on Applications of Laser Anemometry to Fluid Mechanics, Lisbon, Portugal*, 1988.

[57] Simonin, O., Barcouda, M., Flow through staggered tube bundle – ERCOFTAC Classic Collection Database, 1986, [Online]. http://cfd.mace.manchester.ac.uk/ercoftac/doku.php?id=cases:case078 (Accessed Date: January 24, 2024).

[58] Paul, S., Ormiston, S., Tachie, M., Experimental and numerical investigation of turbulent crossflow in a staggered tube bundle. *International Journal of Heat and Fluid Flow*. Vol.29, No.2, pp. 387-414, 2008.

[59] Johnson, R.W., Modeling strategies for unsteady turbulent flows in the lower plenum of the VHTR. *Nuclear Engineering and Design*. Vol.238, No.3, pp. 482-491, 2008.

[60] Ridluan, A., Tokuhiro, A., Benchmark simulation of turbulent flow through a staggered tube bundle to support CFD as a reactor design tool. part I: SRANS CFD simulation. *Journal of Nuclear Science and Technology*. Vol.45, No.12, pp. 1293-1304, 2008.

[61] Ridluan, A., Tokuhiro, A., Benchmark simulation of turbulent flow through a staggered tube bundle to support CFD as a reactor design tool. part II: URANS CFD simulation. *Journal of Nuclear Science and Technology*. Vol.45, No.12, pp. 1305-1315, 2008.

[62] Rollet-Miet, P., Laurence, D., Ferziger, J., LES, and RANS of turbulent flow in tube bundles. *International Journal of Heat and Fluid Flow*. Vol.47, No.14-16, pp. 3057-3071, 1999.

[63] Benhamadouche, S., Laurence, D., LES, coarse LES, and transient RANS comparisons on the flow across a tube bundle. *International Journal of Heat and Fluid Flow*. Vol.24, pp. 470-479, 2003.

[64] Minelli, G., Krajnovi´c, S., Basara, B., LES, and PANS of turbulent flow through a staggered tube bundle. in: Fluids Engineering Division Summer Meeting, Vol. 58059, *American Society of Mechanical Engineers*, p. V01BT12A009, 2017.

[65] Moulinec, C., Pourquie, M., Boersma, B., Buchal, T., Nieuwstadt, F., Direct numerical simulation on a cartesian mesh of the flow through a tube bundle. *International Journal of Computational Fluid Dynamics*. Vol.18, No.1, pp. 1-14, 2004.

[66] Linton, D., and Thornber, B., Direct numerical simulation of transitional flow in a staggered tube bundle. *Physics of Fluids*. Vol.28, No.2, pp. 024111, 2016.

[67] Bruel, P., Florenciano, J.-L., Kousksou, T., Lederlin, T., A test facility for assessing simulations of jets in cross flow configurations, *in Proceedings of the Ninth International ERCOFTAC Symposium on Engineering Turbulence Modelling and Measurements*, Thessaloniki, Greece, hal-00768340, 2012.

[68] Florenciano, J.-L., Study of the response of a flow with wall mass transfer to acoustic forcing (Étude de la réponse d'un écoulement avec transfert pariétal de masse à un forçage acoustique). Phd thesis (in French), University of Pau and Pays Adour, 2013, [Online]. https://www.theses.fr/2013PAUU3013 (Accessed Date: January 24, 2024).

[69] Teixeira, G.S., De Campos, M.D., Best Practice Guidelines on the Ansys in Building Wind Action Applications. *WSEAS Transactions on Fluid Mechanics*, Vol.18, pp. 114-122, 2023, https://doi.org/10.37394/232013.2023.18.12.

[70] Patankar, S.V., Spalding, D.B., A calculation procedure for heat, mass and momentum transfer in three-dimensional parabolic flows. *International Journal of Heat and Mass Transfer*, Vol.15, pp. 1787-1806, 1972.

[71] Grioni, M., Elaskar, S., Bruel, P., Mirasso, A., Comparison of velocity-pressure coupling algorithms for unsteady flow problems around a circular cylinder (Comparación de algoritmos de acoplamiento velocidad-presión para problemas no estacionarios del flujo alrededor de un cilindro circular). *2022 IEEE Biennial Congress of Argentina (ARGENCON), Published in IEEE Xplore*, pp. 1-8, 2022.

[72] Van Doormaal, J., Raithby, G., Enhancements of the simple method for predicting incompressible fluid flows. *Numerical Heat Transfer*, Vol.7, No.2, pp. 147-163, 1984.

[73] Issa, R. I., Solution of the implicitly discretized fluid flow equations by operator splitting. *Journal of Computational Physics*, Vol.62, No.1, pp. 40-65, 1986.

[74] Akoz, M. S., Sahin, B., Akilli, H., Flow characteristic of the horizontal cylinder placed on the plane boundary. *Flow Measurement and Instrumentation*. Vol.21, No.4, pp. 476-487, 2010.

[75] Ozdil, N. F. T. y Akilli, H., Flow comparison around horizontal single and tandem cylinders at different immersion elevations. *Ocean Engineering*, Vol.189, pp. 106352, 2019.

[76] Duffal, V., de Laage de Meux, B., Manceau, R., Development and validation of a new formulation of hybrid temporal large-eddy simulation. *Flow, Turbulence and Combustion*, Vol.108, pp. 1-42, 2022.

[77] Mehta, M., Manceau, R., Duffal, V, de Laage de Meux, B., An active hybrid Reynolds-Averaged Navier-Stokes/Large Eddy Simulation approach for grey area mitigation. *Physics of Fluids*, Vol. 35, No.12, 125116, 2023.

Contribution of Individual Authors to the Creation of a Scientific Article (Ghostwriting Policy)

The authors equally contributed to the present research, at all stages from the formulation of the problem to the final findings and solution.

Sources of Funding for Research Presented in a Scientific Article or Scientific Article Itself

This work has been supported for the Projects ECOS Sud-MinCyT cofinanced by Ministère de l'Europe et des Affaires Étrangères (MEAE) and the Ministère de l'Enseignement Supérieur et de la Recherche et de l'Innovation (MESRI) on the French side and by Ministry of Science, Technology and Innovation on the Argentine side, CONICET-PUE-IDIT, "Vulnerability of infrastructure and physical environment associated with fuel transportation and storage", FONCyT-PICT-2017 "Study of the structural vulnerability of fuel storage tanks and pipes due to loads generated by wind and explosions", CONICET-PIP-GI "Effects of wind, explosions, and fire in fuel storage tanks", the National University of Córdoba "Development and application of theoretical, numerical, experimental and computational codes in fluid mechanics and chaotic intermittency" and the National University of Cuyo Project 06/B050-T1, "Numerical models for the wind action on the layout of circular cylindrical structures with different diameters".

Conflict of Interest

The authors have no conflicts of interest to declare.